Elastic energy release due to domain formation in the strained epitaxy of ferroelectric and ferroelastic films

W. Pompe,[a),b)] X. Gong,[c)] Z. Suo,[c)] and J. S. Speck[a)]
College of Engineering, University of California, Santa Barbara, California 93106

(Received 29 April 1993; accepted for publication 2 August 1993)

Twin related domain formation is examined as a strain relaxation mechanism for a heteroepitaxial tetragonal film on a cubic substrate. Elastic relaxations are calculated for a single twin band in which the c axis of the tetragonal domains is either related by a 90° rotation about an axis in the plane of the film or by a 90° rotation about the surface normal. In all cases, the strain energy change is evaluated for both the film and the substrate. A domain pattern map is developed that predicts single domain and multiple domain fields depending on the relative misfit strains and domain wall energy. The concept of a critical thickness, h_c, for domain formation is developed. For cases in which the c axis is rotated 90° about an axis in the plane of the film, the critical thickness depends only on the relative coherency strain between the substrate and film and the ratio of the domain wall energy to the stored elastic energy. For the case of a pattern consisting of energetically equivalent domains with the c axis in plane, the equilibrium distance of multiple domains is derived. For such multiple domains, a minimum wall separation distance exists that depends nonlinearly on the film thickness.

INTRODUCTION

In this article, twin related domain formation is examined as a mechanism of strain energy release in the heteroepitaxial growth of thin films. For this to be possible, there must be at least two possible orientations (variants or twins) in which the strained film can align with respect to the substrate. This problem is motivated by current activity in the growth of thin film ferroelectrics[1] and thin film ferroelastics.[2] Domains must be considered as a strain relaxation mechanism for heteroepitaxial tetragonal ferroelectrics such as lead titanate or barium titanate on single crystal cubic substrates such as strontium titanate. During the past several years, great progress has been made in the epitaxial growth of oxides on other oxides and on semiconductors.[1,3–6] Much of this work has been driven by the need for effective buffer layers for high temperature superconductors, although it is now recognized that these buffer layers can also be templates for the growth of ferroelectrics and ferroelastics. The recent work of Ramesh *et al.* has demonstrated that epitaxial metallic oxide/ferroelectric/metallic oxide heterostructures for high storage capacitors and memory applications have an ~ 6 order of magnitude improvement in aging and fatigue behavior over heterostructures using conventional metal electrodes.[1,7] This marked improvement has been attributed to either the epitaxial nature of the ferroelectric/electrode interface or the electron affinity across the interface. Given the tremendous potential for ferroelectric devices, the tools for designing favorable domain structures, which differ with engineering applications, must be developed. For instance, periodically poled $LiNbO_3$ striplines is a possible application of elastically stabilized domain patterns.[8] Further, the stability of monovariant films is a critical issue for ferroelectric applications such as sensors or memory. Therefore, not only the formation of periodic domain arrangements, but also single embedded domain segments requires study.

Twin formation has long been recognized as a mechanism of reducing elastic strain energy in constrained phase transformations. Domain formation has been explicitly addressed for coherent precipitation and martensitic phase transformations. Roytburd recognized that domains could provide a mechanism for strain energy release in thin film epitaxy.[9,10] For periodic domain structures, Roytburd estimated the total energy decrease due to domain formation including energy relaxation resulting from a short-range stress field near the film/substrate interface.

Constrained diffusionless phase transformations in the bulk have similarities to phase transformations in thin film epitaxy. In diffusionless *bulk solid-solid phase transformations*, the elastic constraints are largely associated with shape compatibility: the transformed region must fit as closely as possible into the volume previously occupied by the parent phase. Thus, in bulk transformations twin formation is driven by diminishing the stored elastic energy due to large shape changes in both the matrix and the transformed phase; this process is schematically illustrated in Fig. 1. The elastic constraints for solid state phase transformations in epitaxial films are similar to those for bulk materials near the transformed phase/parent phase interface, this region in lightly shaded in the right panel of Fig. 1. *Lattice-matched epitaxy* provides a continuous elastic constraint for the thin film in two dimensions, the film may freely relax in the surface normal direction. The elastic constraint is achieved by matching the two-dimensional film periodicity to the two-dimensional periodic potential of the substrate. Therefore, elastic relaxations can only be concentrated in the film and substrate near discontinuities

[a)]Department of Materials.
[b)]Max-Planck Research Group "Mechanics of Heterogeneous Solids," Dresden, Germany.
[c)]Department of Mechanical and Environmental Engineering.

 0021-8979/93/74(10)/6012/8/$6.00

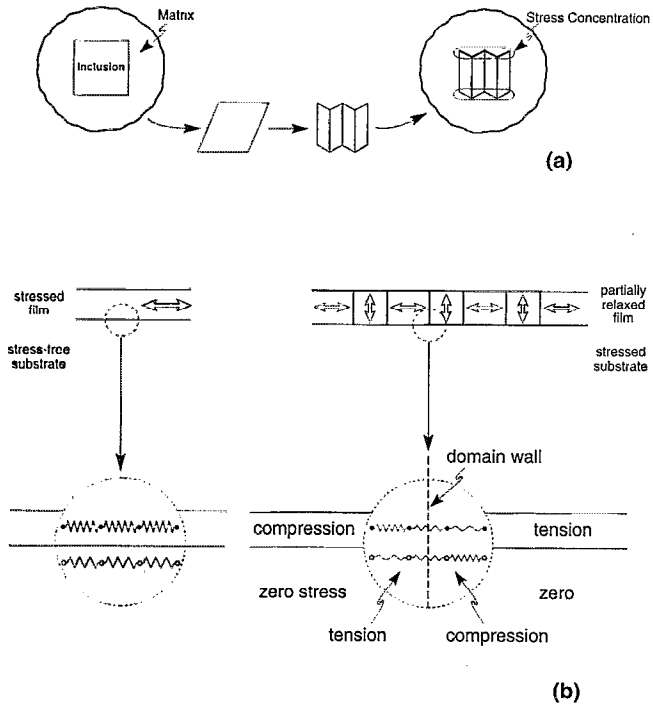

FIG. 1. Schemes of constrained phase transformations. (a) Bulk solid-solid phase transformation with stress relaxation due to shape accommodation by twinning. (b) Solid state phase transformations in epitaxial films with stress relaxation near domain boundaries.

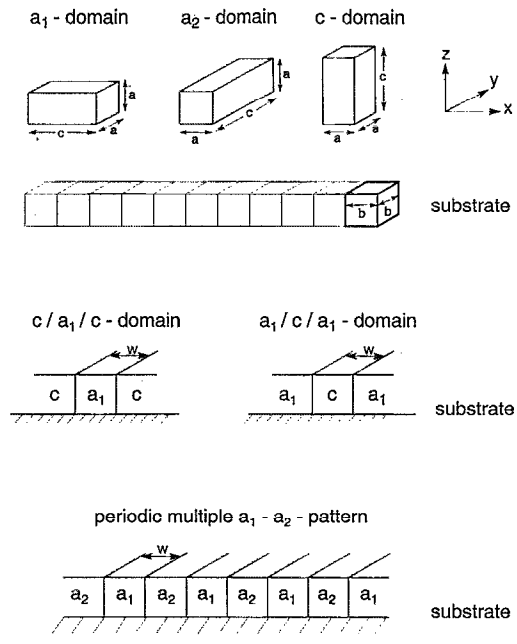

FIG. 2. Characteristic configurations of multivariant tetragonal domains on an (001) cubic substrate.

such as edges or domain boundaries, as demonstrated in extensive elasticity calculations by Hu[11] and Freund and Hu.[12]

It is the aim of the following model to derive exact solutions for the formation of additional domains in strained epitaxial films. It is essential to calculate the stability range of both single embedded and multiple domain assemblies. It will be shown that long range stress relaxations are important for both single embedded domains and also multiple domains. The concept of critical thickness for domain formation is also developed. We draw the analogy to calculations of critical thickness for misfit dislocation generation (see Ref. 13 for an excellent overview of the field) which consider the advance of a single threading segment while leaving behind a misfit segment—the stability of a single strain relieving entity is considered and this is the motivation for studying energy release in the formation of a single embedded twin band.

DEFINITION OF THE PROBLEM AND PHYSICAL MODEL

Consider the strained epitaxy of a thin tetragonal film on a cubic substrate. Domain formation is driven by minimizing the stored elastic energy, and in ferroelectrics, by additionally reducing the electrostatic energy. In ferroelectrics, the polarization energy is reduced by the forming 180° domains. To first order, the elastic effects associated with 180° boundaries are negligible. Thus, the elastic and electrostatic problem can be decoupled for 180° boundaries. In the case of 90° boundaries, the normal component of the polarization vector must be conserved across a boundary for an ideal crystal; otherwise the boundary will have a net charge and a high energy. For real crystals, charges at domain boundaries may be partially compensated by aliovalent dopants and charged point defects. Internal charge compensation is difficult to assess. For the sake of simplicity of the elasticity analysis, we consider 90° boundaries that are normal to the film/substrate interface and the domain boundary energy will be estimated by the twin boundary energy. We believe that the elastic effects of normal and inclined boundaries qualitatively show the same behavior.

The film thickness is h and the domain boundaries are taken to be perpendicular to the interface. The x and y axes lie in the plane of the interface. The lattice parameter of the substrate square lattice is b and the lattice parameters of the film are a and c. The coordinate system used is shown in Fig. 2. We have to distinguish three different domain orientations. For one orientation, referred to as the c domain in the following, the (001) plane of the tetragonal crystal is aligned along the interface with the substrate. Far from any lateral interfaces, the misfit strains of this domain are given as $\epsilon_{xx}=\epsilon_{yy}=\epsilon_a=(b-a)/b$. Additionally, the two variants of the film in which the (100) plane lies in the interface are relevant. Variant 1 of the a domain has misfit strains $\epsilon_{xx}=\epsilon_c=(b-c)/b$, $\epsilon_{yy}=\epsilon_a$ and will be referred to as the a_1 domain. For the variant 2 of the a domain, we select an orientation with misfit strains $\epsilon_{xx}=\epsilon_a$, $\epsilon_{yy}=\epsilon_c$ and refer to this domain as a_2. Before developing a full mathematical model for the strain relaxations in both the film and the substrate due to a single twin band, some straightforward physical concepts are presented to provide a conceptual framework for the problem.

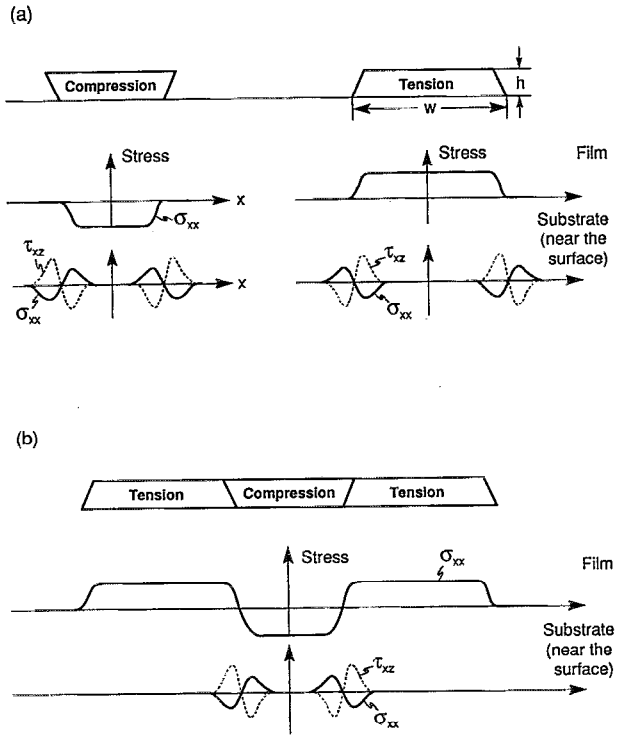

FIG. 3. Physical model of stress distribution in a thin film and the substrate. (a) Thin film islands of width w that are under compression or tension due to epitaxial constraints. (b) Continuous film with a bandlike domain structure of changing coherency.

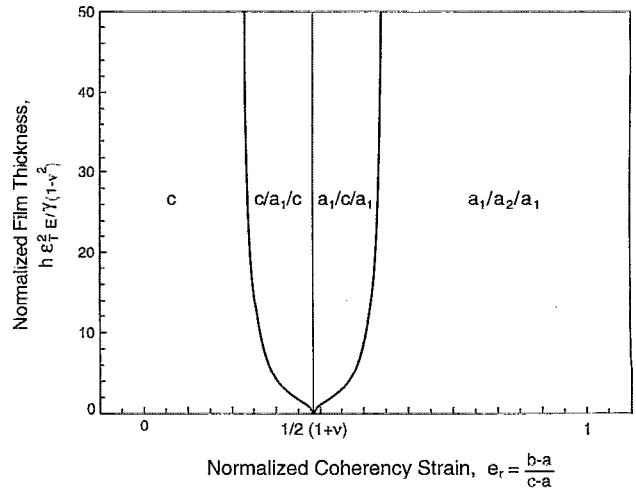

FIG. 4. Equilibrium diagram of domain patterns based on the relative coherency strain e_r and the normalized film thickness.

Domain patterning can be understood qualitatively as follows. First consider monovariant films, one in tension (case I) and the other in compression (case II). The substrate is semi-infinite and therefore free of stress. Now consider islands of the strained epitaxial film on the substrate, Fig. 3(a). At the island boundaries the film cannot sustain a normal stress σ_{xx}, and the strain in the film relaxes at the island boundaries. This process occurs at the expense of strain in the substrate. Bringing islands together with different epitaxial misfits leads to domain boundaries, as shown in Fig. 3(b). The material near the boundary acts as a displacement "absorber." The normal stress in the film near the domain boundaries are diminished; however, substrate stresses are induced near the domain walls. This process of mutual elastic accommodation between tensile and compressive islands provides the basis for domain patterning as a mechanism of strain energy release in multivariant thin films.

EQUILIBRIUM DOMAIN STRUCTURES

The following simplifications will be invoked to calculate the strain energy. The film and the substrate are taken to be elastically isotropic and homogeneous with Young's modulus E and Poisson's ratio ν. (A value $\nu=0.3$ will be used in the plots.) Each domain is long in the y direction compared to the film thickness, so that stresses everywhere are invariant with respect to y. Here we analyze the equilibrium domain patterns that result from the competition between the strain energy reduction and the domain wall energy. As such, other energy varying mechanisms are assumed to be negligible. We do not treat nucleation of domains or kinetics of domain wall motion. However, from the stability arguments we can derive the driving forces for such processes. Thus, both the film thickness h and domain width w are regarded as variables in minimizing the combined strain and domain wall energy.

Our analysis indicates that a diagram of equilibrium domain patterns may be developed by using two nondimensional variables: the relative coherency e_r defined by the ratio of one misfit strain, $\epsilon_a=(b-a)/a$, to the tetragonality strain, $\epsilon_T=(c-a)/a$

$$e_r=\frac{b-a}{c-a} \tag{1}$$

and the ratio of the strain energy over the domain wall energy

$$hE\epsilon_T^2/\gamma, \tag{2}$$

where γ is the specific domain wall energy, and E is the Young's modulus of the film. We now develop an equilibrium diagram for domain stability, the results of which are presented in Fig. 4. Qualitative features in the diagram are discussed below, followed by a detailed analysis in the next section.

When $b<a$, or $e_r<0$, all variants are under biaxial compression; the film tends to make an a-to-c switch to stabilize as a single c domain. When $b>c$, or $e_r>1$, all variants are under biaxial tension; the film tends to make a c-to-a switch to stabilize with alternating a_1 and a_2 domains. A value $e_r=e_c$ exists where the epitaxy causes the same strain energy in the a and c variants. This is the vertical line in Fig. 4; the c variant dominates on the left, and the a variants dominate on the right. A multidomain region appears near $e_c-\Delta e \leqslant e_r \leqslant e_c+\Delta e$. For example, when $e_r<e_c$, the strain energy of a large c domain may be diminished by embedding small a domains. Similarly,

when $e_r > e_c$, small c domains may be stable within a large a domain. The mechanism is efficient for thicker films, because the strain energy relaxation is volumetric in nature whereas the domain wall energy scales with area. Thus, the range of stable multiple domain structures increases with increasing film thickness.

To simplify some of the calculations, the film is sandwiched between two thick substrates, so that Green's functions for an infinite space under plane strain conditions can be used. These simplifications notwithstanding, we emphasize the broad features of the equilibrium diagram, and the trend of the domain pattern fields should be of general validity.

MONOVARIANT FILMS

Epitaxial, monovariant films of either type a or c provide the reference for the energy change to be considered in the later sections. Because the film is much thinner than the substrate, the substrate is undeformed and, to match the undeformed lattice of the substrate, the film is strained by

$$\epsilon_a = \frac{b-a}{a}, \quad \epsilon_c = \frac{b-c}{c}. \tag{3}$$

The stresses in the film for the c variant are determined by Hooke's law:

$$\sigma_{xx} = \sigma_{yy} = \frac{E}{1-\nu}\epsilon_a, \quad \sigma_{zz} = 0 \tag{4}$$

and for the a_1 variant:

$$\sigma_{xx} = \frac{E}{(1-\nu^2)}(\epsilon_c + \nu\epsilon_a),$$
$$\sigma_{yy} = \frac{E}{(1-\nu^2)}(\epsilon_a + \nu\epsilon_c), \quad \sigma_{zz} = 0. \tag{5}$$

The strain energy per unit volume can be readily computed for the c variant:

$$\eta_c = \frac{E}{1-\nu}\epsilon_a^2 \tag{6}$$

and for the a_1 variant

$$\eta_a = \frac{E}{2(1-\nu^2)}(\epsilon_a^2 + \epsilon_c^2 + 2\nu\epsilon_a\epsilon_c). \tag{7}$$

Note that the a_1 and a_2 variants have the same strain energy. It follows by equating the above energy densities that both variants are energetically equivalent when

$$e_c = \frac{\epsilon_a}{\epsilon_a - \epsilon_c} = \frac{1}{2(1+\nu)}, \tag{8}$$

with $\epsilon_a/(\epsilon_a - \epsilon_c) = e_r[1/(1+\epsilon_c)] \simeq e_r$ for small strains. This approximation of small strains will be made throughout this paper. This is the vertical line in Fig. 4, $e_c = 0.385$ (for $\nu = 0.3$). The c variant has the lower strain energy on the left of the line, and the a variants have the lower strain energy on the right.

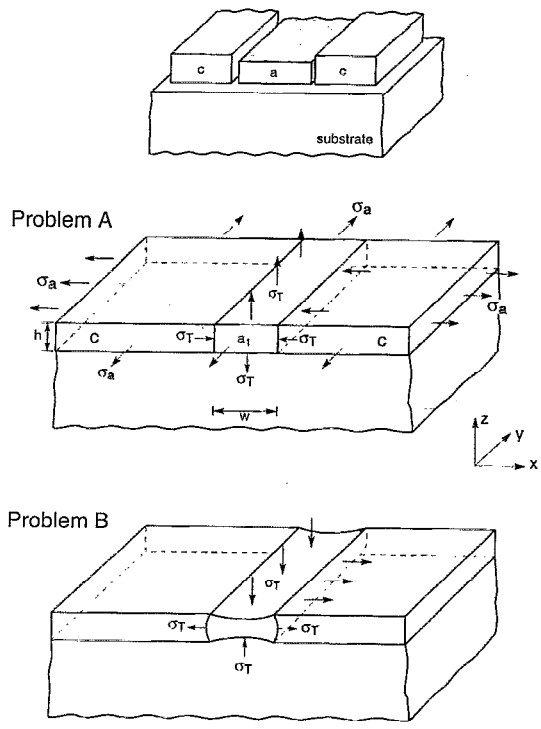

FIG. 5. Micromechanical model of an embedded domain band. In problem A clamping tractions are applied to match the variants and the substrate. In problem B tractions σ_T in the opposite directions are applied to remove σ_T in problem A.

FORMATION OF DOMAIN BANDS

When $e_r < e_c$, even though the c variant has a lower strain energy than the a variant, a small a domain may emerge in a large c domain to reduce the elastic energy in the film. This is done at the expense of adding the domain walls and deforming the substrate. Proper energy accounting requires that the elasticity problem be solved rigorously. In what follows a specific configuration, a long a_1 band in a large c domain (Fig. 2), is analyzed. We will determine (i) the equilibrium band width, and (ii) the stability range for domain formation. The a_1 bands, disrupting a perfect c-variant film, bear much similarity to other strain-relaxing mechanisms in thin films. Familiar examples include misfit dislocations[13] and channeling cracks.[14]

The lattice misfits among the variants and the substrate cause a complicated stress field. We solve the elasticity problem by the linear superposition of problems A and B in Fig. 5. Consider problem A first. Starting from the unbonded a_1 band, c domain, and substrate, the a_1 band is deformed to match the three-dimensional lattice of the c domain. The operation compresses the c axis and extends one of the a axis of the a_1 band by a traction of magnitude

$$\sigma_T = \frac{E\epsilon_T}{1+\nu}. \tag{9}$$

The bivariant film is then stressed biaxially by σ_a to match the lattice of the substrate, where

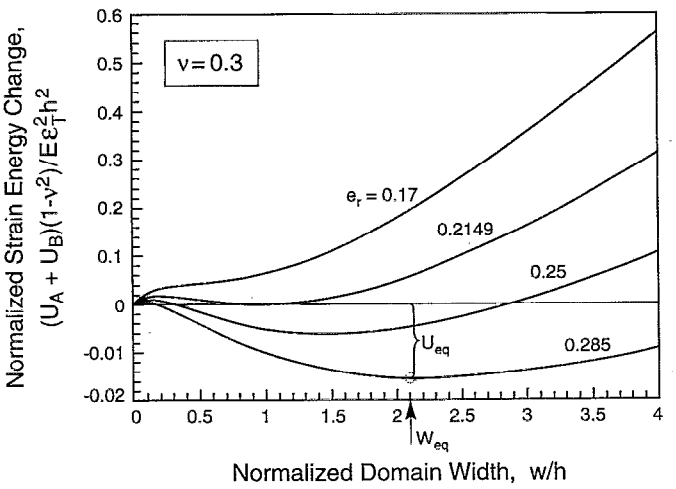

FIG. 6. Calculated difference in the strain energies between a large c domain with and without the a_1 band for various relative coherency strains e_r. The equilibrium band width and the associated reduction in the strain energy are indicated for one curve.

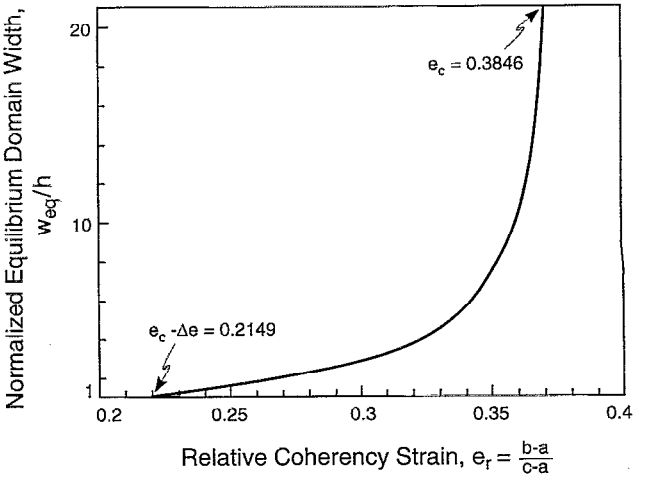

FIG. 7. Dependence of the equilibrium domain width of a $c/a_1/c$ configuration on the relative coherency strain e_r (the configuration is favored in the range $e_c-\Delta e<e_r<e_c$).

$$\sigma_a=\frac{E\epsilon_a}{1-\nu}. \tag{10}$$

The two operations result in uniform stresses given by Eq. (4) in the c domain, and by

$$\sigma_{xx}=\sigma_a-\sigma_T, \quad \sigma_{yy}=\sigma_a, \quad \sigma_{zz}=\sigma_T \tag{11}$$

in the a_1 band; the substrate remains undeformed. Compared with the strain energy per unit domain band length in a c monovariant, problem A increases the strain energy by

$$U_A=\frac{E}{1-\nu}\epsilon_T^2hw\left(\frac{1-\nu}{1+\nu}-e_r\right). \tag{12}$$

Problem A differs from the original problem only in one aspect: the clamping tractions σ_T that prevent relaxation. Upon removing the tractions, the lattice mismatches deform the system. On the basis of linear superposition, the displacement field, after removing σ_T from problem A, is the same as that induced solely by the negative tractions without the lattice mismatches, as illustrated by problem B. Because the tractions in problem A and the displacements associated with their removal are in opposite directions, the work reduces the strain energy of the system. Thus, the change in the strain energy scales as

$$U_B=-\epsilon_T^2h^2Eg\left(\frac{w}{h}\right), \tag{13}$$

where g is a dimensionless function of w/h. The displacements in problem B is obtained by integrating Green's functions; U_B is the work done per unit band length by tractions σ_T through the associated displacements. Both are described in the Appendix.

The difference in the strain energies in a large c domain with and without the a_1 band, U_A+U_B, is shown in Fig. 6, varying with both w and e_r. Two types of behaviors emerge. When $e_r<e_c-\Delta e=0.2149$ (for $\nu=0.3$), embedding an a_1 band of any w increases the strain energy, so that the c monovariant is favored. When $e_c-\Delta e<e_r<e_c$, an a_1 band over a limited range of width decreases the strain energy. The equilibrium band width w_{eq} minimizes the strain energy, which is indicated in Fig. 6 for one value of e_r. Also indicated is U_{eq}, the strain energy reduction due to embedding the a_1 band.

Plotted in Fig. 7 is the equilibrium band width associated with the strain energy minima. As the band width varies, the domain wall area remains constant so that the equilibrium domain width is independent of the domain wall energy. Other quantities being fixed, the band width increases as either the film/substrate lattice misfit increases, or the tetragonality of the film decreases. Embedding an a_1 band into a c domain adds two domain walls. The a_1 band forms when the strain energy reduction U_{eq} compensates the domain wall energy, i.e.,

$$U_{eq}+2\gamma h=0. \tag{14}$$

Because U_{eq} scales as h^2, this condition defines a critical film thickness, below which the a_1 band is unstable, and the film stabilizes as a c monovariant. The critical thickness, obtained from the calculated U_{eq}, is plotted in Fig. 4, separating two regions of equilibrium domain patterns: the c monovariant prevails below the curve, and a_1 bands form above the curve.

When $e_r>e_c$, an epitaxial a monovariant has a lower strain energy than the c monovariant. Similar calculations lead to the symmetric pattern in Fig. 4 which separates the region of coexisting a and c domains from the region of only a variants. In a normalized plot of Fig. 8, similar to Fig. 6, we show the total energy change with both the elastic energy change and the interfacial energy change. Since the model of embedded domains does not include domain nucleation, the energy offset at $w/h=0$ is due to the formation of two domain boundaries. For $0<w/h<w^*/h$, the change in normalized total energy is positive because of restricted elastic relaxation in the film.

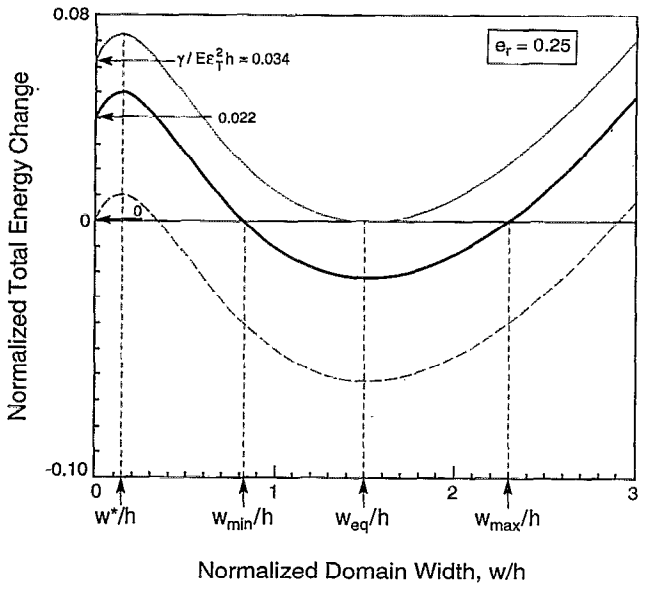

FIG. 8. Dependence of the total energy change $[U_{tot}(1-\nu^2)]/E\epsilon_T^2 h^2$, on the domain width w and the domain wall energy for a single $c/a_1/c$ configuration. With decreasing domain wall energy or increasing film thickness, domain formation is energetically favored (for $e_r=0.25$ the critical ratio is given by $\gamma/(Eh\epsilon_T^2)=0.34$).

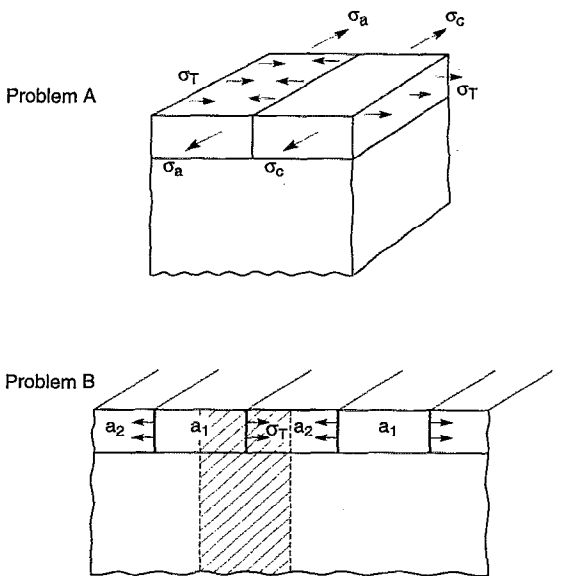

FIG. 9. Micromechanical model of equivalent variants. In problem A different biaxial tractions are applied on the two variants to match the undeformed lattice of the substrate, resulting in unbalanced traction on the domain walls, σ_T. In problem B tractions in the negative directions are applied.

That is, the "displacement absorbing" domain has insufficient width and the energy is dominated by strain in the substrate. For $w^*/h < w/h < w_{min}/h$ the energy relaxation in the film dominates the slope of the curve, and domain formation in this range is thermodynamically unfavorable due to wall energy and substrate relaxation; however, preexisting domains may coarsen to the normalized width w_{eq}/h. Thus, this is a region of extended stability. For $w_{min}/h < w/h < w_{max}/h$, the existence of domains is thermodynamically favored and isolated domains will strive to adjust their normalized widths to w_{eq}/h.

PATTERNING OF EQUIVALENT VARIANTS

Now consider the region in the equilibrium diagram where the c variant completely disappears. Epitaxial films of single a_1 or a_2 variants have the same strain energy. We will show that the film stabilizes with alternating a_1 and a_2 domains—that is, a monovariant film, say of a_1 type, is unstable for any film thickness. Our conclusion thus differs from that of Roytburd[10] and the differences in approaches will be noted.

The two variants are assumed to form alternating bands with the same width w (Fig. 2). A monovariant film corresponds to infinite w/h. The two variants accommodate each other, reducing the strain energy, causing a complicated stress distribution. The elasticity problem is solved by superposing problems A and B in Fig. 9. In problem A, each domain is biaxially stretched by tractions of magnitude in Eq. (5) to match the lattice of the undeformed substrate. It follows that unbalanced tractions exert on the domain walls, with magnitude

$$\sigma_T = \frac{E}{(1+\nu)}\epsilon_T. \tag{15}$$

Each domain has the identical strain energy density given by Eq. (7), and the substrate remains undeformed.

Upon removing σ_T from problem A, the domain walls displace in the direction opposite to the tractions. The displacements are computed from problem B by integrating Green's functions, and the work done in removing σ_T is computed by integrating the displacements. The strain energy change per unit band length in the section of width w, shaded in Fig. 9, scales as

$$U \approx -h^2 E\epsilon_T^2 f\left(\frac{w}{h}\right), \tag{16}$$

where f is a dimensionless function of w/h. The computed result is plotted in Fig. 10. Everything else being fixed, the strain energy reduction U diverges as $\ln(w/h)$ when w/h is large.

$$\lim_{w/h\to\infty} f\left(\frac{w}{h}\right) = \frac{3-4\nu}{8\pi(1-\nu^2)}\ln\left(\frac{w}{h}\right) + \frac{1-2\nu}{2\pi(1-\nu^2)}. \tag{17}$$

The asymptote can be understood as follows: as w/h becomes large, the stress field far away from the applied traction σ_T is the same as that due to a concentrated force. Consequently, the stress decays as $1/r$ with distance r, and the strain energy has a logarithmic asymptote. The significance of the divergent energy reduction will become apparent below.

Including both the change in the strain energy and the domain wall energy (with respect to a monovariant), the average energy change in the system, per unit length in both x and y directions, is

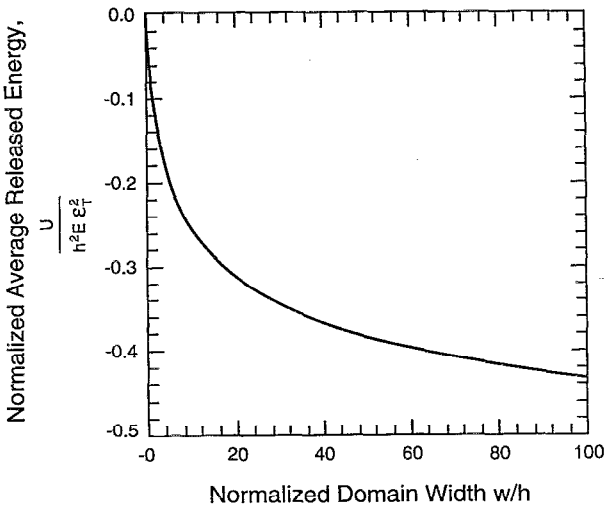

FIG. 10. Strain energy reduction due to patterning of equivalent domains.

$$\frac{(U+\gamma h)}{w}. \tag{18}$$

The computed results are plotted in Fig. 11, varying with the domain width and the domain wall energy. Note that the "energy change" is with respect to the strain energy in an a_1 monovariant. When w/h is small, the domain wall energy dominates so that the energy change is positive. When w/h exceeds some finite value, the strain energy reduction dominates so that the energy change becomes negative. The average energy becomes indistinguishable from that of a monovariant film for large w/h. Consequently, *an equilibrium domain width exists for any film thickness* which minimizes the total energy below the strain

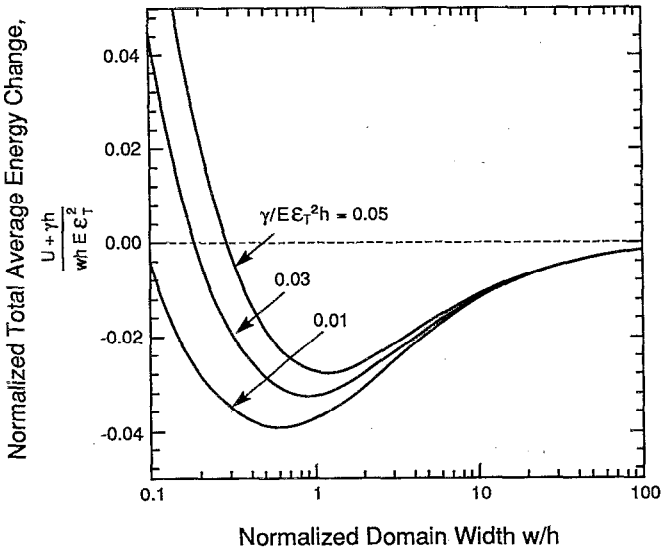

FIG. 11. Total energy changes as a result of the competition between domain wall energy and strain energy reduction due to patterning (note the log-linear scales employed).

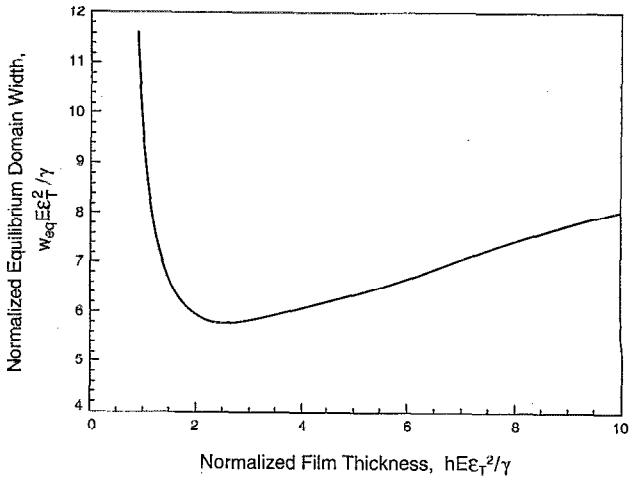

FIG. 12. Equilibrium domain width of alternating equivalent variants.

energy of the a monovariant. That is, *the alternating pattern is always energetically favored over an a monovariant.*

Roytburd used an approximate formula for the strain energy in studying a similar problem.[10] The formula is obtained when $w/h \ll 1$ and introduces large errors when the domain width is comparable to, or larger than, the film thickness. The formula leads to the erroneous conclusion that a critical thickness exists, below which a monovariant, such as the a_1 type, is stable.

The equilibrium domain width that minimizes the energy is plotted in Fig. 12. Other quantities being fixed, a minimum domain width exists as the film thickness changes. At small film thicknesses, the equilibrium domain width increases exponentially as the film thickness decreases. This phenomenon is absent from Roytburd's estimate, and is due to the elastic interaction among the domains and the substrate over distances exceeding the film thickness. For very large film thickness the equilibrium domain size scales as

$$w_{\text{eq}} \propto \left(\frac{h\gamma}{E\epsilon_T^2}\right)^{1/2}, \quad \frac{hE\epsilon_T^2}{\gamma} \gg 1. \tag{19}$$

This recovers the Roytburd estimate. As evident from Fig. 12, this asymptote differs appreciably from the complete solution in the plotted region, as is valid only when $hE\epsilon_T^2/\gamma > 10$.

CONCLUDING REMARKS

The current paper has treated strain relaxation only by domains. A future paper will incorporate the role of misfit dislocations in strain relaxation of epitaxial ferroelectrics. By minimizing the combined strain energy and domain wall energy, we have developed a diagram of equilibrium domain patterns for a tetragonal film epitaxially grown on a cubic substrate (Fig. 4). The c and a variants dominate over the two sides of the diagram, separated by a critical value of the misfit parameter, $e_r = e_c$. When $e_c - \Delta e < e_r < e_c$, a critical film thickness exists below which the film stabilizes as a perfect c variant. Above the critical

thickness, bands of a_1 variant traverse the c variant to reduce the strain energy. When $e_c < e_r < e_c + \Delta e$, a critical film thickness exists below which the c variant disappears completely. In this region, the film can only stabilize with alternating a_1 and a_2 domains, but not a monovariant. The equilibrium domain bands are computed. The dependence of the stability ranges on the relative coherency strain of the film/substrate system opens a way for the engineering of domain configurations. Many parameters may be varied to control the domain structure, including choice of substrate, and alloying the substrate and film to control lattice parameters.

ACKNOWLEDGMENTS

We would like to thank Professor F. F. Lange and Professor A. G. Evans for encouragement and several enlightening discussions. The work of J.S. and W.P. was partially supported by the MRL Program of the National Science Foundation under Award No. DMR-9123048. The work of X.G. and Z.S. was supported by the National Science Foundation through Grant No. MSS-9258115, and by the Office of Naval Research through Contract No. N00014-93-1-0110.

APPENDIX

An outline is provided here for Green's functions for an infinite elastic body under plane strain conditions, and the procedures employed to compute the work done in removing tractions in problem A in Figs. 5 and 9. In the coordinates defined in Fig. 13, the Green's functions, i.e., displacements G_x and G_z due to a pair of unit forces in $\pm x$ directions, are written[15]

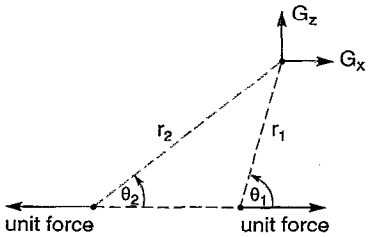

FIG. 13. Coordinates for Green's functions with a pair of unit forces in an infinite space.

$$\beta G_x = (6-8\nu)\ln\left(\frac{r_1}{r_2}\right) + \cos 2\theta_1 - \cos 2\theta_2, \tag{A1}$$

$$\beta G_z = \sin 2\theta_1 - \sin 2\theta_2, \tag{A2}$$

where

$$\beta = 4\pi E \frac{1-\nu}{1+\nu}. \tag{A3}$$

The rigid body translation is set such that both displacements vanish at infinity. The displacement field in problem B in Fig. 5 is obtained by integrating the product of the Green's functions with σ_T through the thickness of the film, i.e., from $z=-h/2$ to $z=h/2$. Green's functions for a pair of unit forces along the y axis are obtained by rotating the above results. The work done by tractions σ_T through the associated displacements, i.e.,

$$\sigma_T \int_{-h/2}^{h/2} u_x(w/2,z)\,dz - \sigma_T \int_{-w/2}^{w/2} u_z(x,h/2)\,dx, \tag{A4}$$

gives the magnitude of U_B in Eq. (13), where u_x and u_z are the displacements calculated in problem B of Fig. 5. Numerical integration is used to obtain the applied work.

The displacement field in problem B in Fig. 9 is obtained by integrating Green's functions, which also involves a sum of an infinite series. The strain energy in the shaded area in Fig. 9 is computed by the traction σ_T on one domain wall through the associated displacement.

[1] R. Ramesh, T. Sands, and V. G. Keramidas, Appl. Phys. Lett. **63**, 731 (1993).
[2] A. Seifert, J. S. Speck, and F. F. Lange, J. Am. Ceram. Soc. **76**, 443 (1993).
[3] D. K. Fork, D. B. Fenner. G. A. N. Connell, J. M. Phillips, and T. H. Geballe, Appl. Phys. Lett. **57**, 1137 (1990).
[4] D. K. Fork, F. A. Ponce, J. C. Tramontana, and T. H. Geballe, Appl. Phys. Lett. **58**, 2294 (1991).
[5] W.-Y. Hsu and R. Raj, Appl. Phys. Lett. **60**, 3105 (1992).
[6] E. Tarsa, J. English, and J. S. Speck, Appl. Phys. Lett. **62**, 2332 (1993).
[7] R. Ramesh, W. K. Chan, B. Wilkens, H. Gilchrist, T. Sands, J. M. Tarascon, V. G. Keramidas, D. K. Fork, J. Lee, and A. Safari, Appl. Phys. Lett. **61**, 1537 (1992).
[8] D. K. Fork, J. J. Kingston, G. B. Anderson, E. J. Tarsa, and J. S. Speck, MRS Symp. Proc. (to be published).
[9] A. L. Roitburd, Phys. Status Solidi A **37**, 329 (1976).
[10] A. L. Roytburd, Mater. Res. Soc. Symp. Proc. **221**, 256 (1991).
[11] S. M. Hu, J. Appl. Phys. **50**, 4661 (1979).
[12] L. B. Freund and Y. Hu, Shear Stress at a Film-Substrate Interface due to Mismatch Strain, (Office of Naval Research Contractor Report No. N 000 14-87-K-0481, 1988).
[13] L. B. Freund, MRS Bull. **17**, 52 (1992).
[14] J. W. Hutchinson and Z. Suo, Adv. Appl. Mech. **29**, 63 (1992).
[15] S. P. Timoshenko and J. N. Goodier, *Theory of Elasticity* (McGraw-Hill, New York, 1951).